that unprecedented environmental changes, most likely related to climatic warming, have occurred since the beginning of the 19th century. Other workers, using different proxy methods, have also indicated recent climatic warming in different arctic regions (*26*, *27*), but our data indicate an earlier (by over a century) start for these changes.

Given the absence of comparable paleolimnological studies from other high-latitude ponds, we cannot yet determine how widespread these changes have been. Any attempts at cataloging pristine arctic assemblages may already be too late, as our data indicate that high-arctic ponds have already changed.

REFERENCES AND NOTES

1. R. A. Kerr, *Science* **212**, 1013 (1981).
2. R. M. Koerner and D. Fisher, *Nature* **295**, 137 (1982).
3. R. McNeely and W. D. Gummer, *Arctic* **37**, 210 (1984).
4. L. A. Barrie *et al.*, *Sci. Total Environ.* **122**, 1 (1992).
5. J. T. Houghton, G. J. Jenkins, J. J. Ephraums, Eds., *Climate Change: The IPCC Scientific Assessment* (Cambridge Univ. Press, Cambridge, 1990).
6. D. W. Gullet and W. R. Skinner, *The State of Canada's Climate: Temperature Change in Canada 1859-1991* (State of the Environment Rep. 92-2, Atmospheric Environment Service, Environment Canada, Ottawa, 1992).
7. J. P. Smol, *Verh. Int. Verein. Limnol.* **23**, 837 (1988).
8. S. S. Dixit, J. P. Smol, J. C. Kingston, D. F. Charles, *Environ. Sci. Technol.* **26**, 23 (1992).
9. W. Blake Jr., *Geol. Surv. Can. Pap.* **77-1C**, 107 (1977).
10. J. Bridgland and J. M. Gillett, *Can. Field Nat.* **97**, 279 (1983).
11. M. S. V. Douglas, thesis, Queen's University (1989).
12. ———, thesis, Queen's University (1993).
13. ——— and J. P. Smol, *Nova Hedwigia Z. Kryptogamenkd.* **57**, 511 (1993).
14. ———, *Arch. Hydrobiol.*, in press.
15. K. E. Duff, M. S. V. Douglas, J. P. Smol, *Nord. J. Bot.* **12**, 471 (1992).
16. T. Nogrady and J. P. Smol, *Hydrobiologia* **173**, 231 (1989).
17. M. S. V. Douglas and J. P. Smol, *J. Phycol.*, in press.
18. W. Blake Jr., *Geol. Surv. Can. Pap.* **78-IC**, 119 (1978).
19. ———, *ibid.* **82-1C**, 104 (1982).
20. The corer was from a design developed by the Snow, Ice, and Permafrost Research Establishment (SIPRE), now the Cold Regions Research and Engineering Laboratory (CRREL).
21. D. J. Conley, *Biogeochemisty* **6**, 161 (1988).
22. W. Blake Jr., *Can. J. Earth Sci.* **29**, 1958 (1992).
23. P. Schledermann, *Crossroads to Greenland* (Komatik Ser. no. 2, Arctic Institute of North America, University of Calgary, Calgary, 1990).
24. J. Blais, personal communication.
25. S. Roy and W. F. Vincent, *Environ. Rev.* **1**, 1 (1993).
26. R. M. Koerner and D. A. Fisher, *Nature* **343**, 630 (1990).
27. R. S. Bradley, *Quat. Sci. Rev.* **9**, 365 (1990).
28. This research was supported by the Natural Sciences and Engineering Research Council of Canada, Polar Continental Shelf Project, Geological Survey of Canada (contribution 12494), Northern Studies Training Program, and the Cape Herschel Project (contribution 50). The ^{210}Pb dating was performed by B. Risto and R. J. Cornett at the Atomic Energy Canada. This paper benefited from comments by R. Bradley, H. J. Birks, R. Scherer, R. Koerner, J. Bourgeois, B. Cumming, and scientists at the Paleoecological Environmental Assessment and Research Laboratory.

2 June 1994; accepted 31 August 1994

Strength of Diamond

Donald J. Weidner, Yanbin Wang, Michael T. Vaughan

The yield strength of diamond is measured under a pressure of 10 gigapascals at temperatures up to 1550°C by the analysis of x-ray peak shapes on diamond diffraction lines in a powdered sample as a function of pressure and temperature. At room temperature, the diamond crystals exhibit elastic behavior with increasing pressure. Significant ductile deformation is observed only at temperatures above 1000°C at this pressure. The differential yield strength of diamond decreases with temperature from 16 gigapascals at 1100°C to 4 gigapascals at 1550°C. Transmission electron microscopy observations on the recovered sample indicate that the dominant deformation mechanism under high pressure and temperature is crystal plasticity.

Diamonds are widely used as indentors as well as cutting, drilling, grinding, and wire-drawing tools that are generally used under high-stress conditions. Diamond anvil cells and large-volume, multianvil apparatus that use polycrystalline diamond compacts are the major instruments for high-pressure–high-temperature research (*1–3*). All of these applications require a knowledge of the strength of diamonds. However, quantitative data for diamond yield strength remain elusive because diamond is so difficult to deform. To measure yield strength, it is generally necessary to apply a force until the material flows, measuring the force and the resulting deformation while separating the effects of fracture from ductile flow. To do this, the deforming apparatus needs to be stronger than the sample; because diamond is the strongest known material, these measurements have been very difficult to accomplish. Therefore, most of the previous strength measurements for diamond have been conducted with indentation (*4*), torsion (*5*), and bending (*6*) techniques. The conversion of these measurements to compressional and tensile strength values is often ambiguous. The heating of diamond at room pressure in excess of 1500°C generally results in extensive graphitization (*7*). Furthermore, ductile deformation in most materials only occurs under sufficient pressures, temperatures, or both (*8*). To determine the ductile deformation of diamond, it is necessary to make the measurements at high temperature and at a pressure within the diamond stability field so that neither brittle failure nor graphitization contributes to the results.

Here we report results on the yield strength of a powdered diamond sample at temperatures up to 1550°C and at a pressure of 10 GPa, conditions that serve both to stabilize the diamond phase of carbon and to provide the driving force to produce deviatoric stresses at grain contacts (*9*). The experiment was conducted with a DIA-type, cubic-anvil, high-pressure apparatus, SAM-85 (*10*). A powdered diamond-polishing compound (Crystallite Corporation, Marina del Ray, California) with an average grain size of 3 μm fills a portion of the sample volume about 0.5 mm long and 1.2 mm in diameter, and powdered NaCl mixed with BN is loaded into the remaining portion of the sample volume. The equation of state of NaCl is used to determine the cell pressure at various temperatures (*11*).

Energy-dispersive x-ray diffraction data are collected at a fixed scattering angle of 10° at the superconducting wiggler beam line (X17B1) at the National Synchrotron Light Source. The x-ray beam is collimated to 100 μm in its vertical dimension and 200 μm in its horizontal dimension. Diffraction spectra of the diamond are collected at the same position in the sample at various temperatures in an energy range up to 100 keV, with a collection time of 300 s. Estimated temperature variation in the diffracting volume is less than 5°C (*12*).

We use the method described in (*9*) to obtain information of stress in the sample from diffraction signals. Under a hydrostatic pressure boundary condition, heterogeneities within the sample along with elastic anisotropy are responsible for generating stresses that vary from grain to grain. The effect of this microscopic deviatoric stress field is the broadening of x-ray diffraction lines, and the amount of line broadening is an indicator of the distribution of longitudinal strain parallel to the diffraction vector (*13*). The width of the diffraction lines is a convolution of the instrument response, sample response function, and the longitudinal elastic strain distribution parallel to the diffraction vector. Using the room pressure and temperature spectra as a reference for zero strain, we calculate the strain distribution in the sample at elevated pressure and temperature as the root-mean-square broadening. By multiplying the strain by an appropriate aggregate elastic modulus [in the experiment we used

Center for High Pressure Research and Department of Earth and Space Sciences, State University of New York, Stony Brook, NY 11794–2100, USA.

the aggregate Young's modulus, 1050 GPa, for diamond (*14*)], we convert the strain to stress. If sufficient deviatoric stress is generated by the loading system to deform the sample plastically, then this stress represents the yield strength of the sample corresponding to a few percent strain. Several criteria have been established to determine whether the deviatoric stress reaches the yield point of the sample (*9*).

During the experiment, the diamond sample was first compressed to 10 GPa and then heated to 1550°C. Figure 1 illustrates the (111) diffraction peak at selected points along this path. During the compression portion of the cycle the diamond diffraction peak broadens asymmetrically, with the large *d*-spacing side of the peak remaining unchanged. This configuration indicates that in the diamond aggregate, some of the grains do not support any of the applied stress. Thus, the pressure is being supported by a subset of the diamond grains that are bridging and not yielding. Figure 2 shows the deviatoric strain determined from the (111) reflection as a function of applied pressure at room temperature and as a function of temperature at 10 GPa. Strains corresponding to both the half peak height and the quarter peak height are indicated. The linear dependence of strain with pressure indicates that the loading process is elastic, thereby demonstrating that neither brittle nor ductile processes are activated.

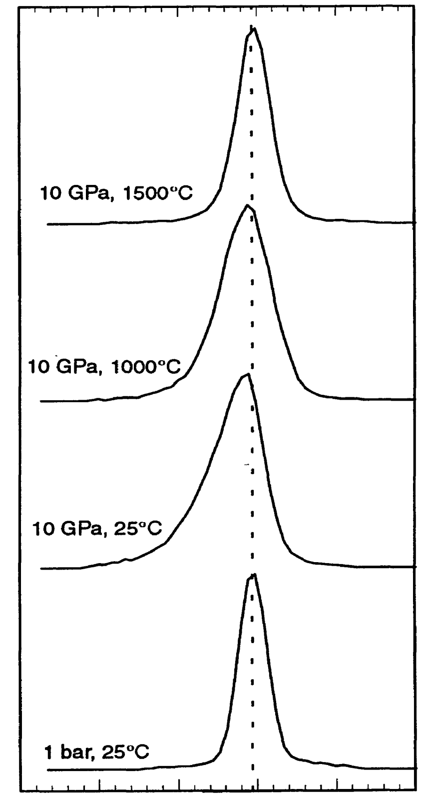

Fig. 1. (111) Diffraction peak (in relative units) of diamond at the indicated pressure and temperature. The initially symmetric peak broadens asymmetrically as pressure is applied. As the sample is heated, the shape remains constant up to 1000°C, above which it narrows and becomes more symmetrical.

As temperature is increased to 1000°C, the shape of the diffraction peak is maintained but moves to higher *d* spacing, indicating the effects of thermal expansion on all of the grains. In this region, there is still no evidence of either ductile or fracture-induced stress relaxation. In fact, the slight negative slope in the strains is due to the pressure decrease with increasing temperature. Furthermore, the constancy of deviatoric strain to 1000°C indicates that the supported deviatoric stress was less than the yield strength of diamond.

Above 1000°C, the peak begins to narrow and becomes symmetric. In this region, the grains that experience high deviatoric stress are yielding and redistributing the stress to the entire sample. Thus, we can estimate the yield strength from the magnitude of the elastic deviatoric strain, as outlined above. The temperature dependence of the yield strength is illustrated in Fig. 3. Because the plastic strain, as given by the amount of strain that relaxes at high temperature, is on the order of 1% of the total strain and the time of the experiment is a few minutes, the strain rate is on the order of 10^{-6} s^{-1}. The deduced strength can be directly compared with that of Knoop hardness data at ambient pressure (*15*). For the sake of comparison, we converted the hardness (H) data of (*10*) to yield-strength values ($\sigma = \sigma_1 - \sigma_2$), based on the empirical relation $H = C\sigma$, with an arbitrarily chosen $C = 3$. For most minerals, C varies between 1 and 5 (*15*). Analyses on three diffraction lines give consistent results. Previous three-point bending data at room pressure and 1800°C (*6*) are also indicated in this figure. Our results are consistent with these previous observations, despite the different experimental techniques, and the new data extend the results for diamond yield strength to lower temperatures.

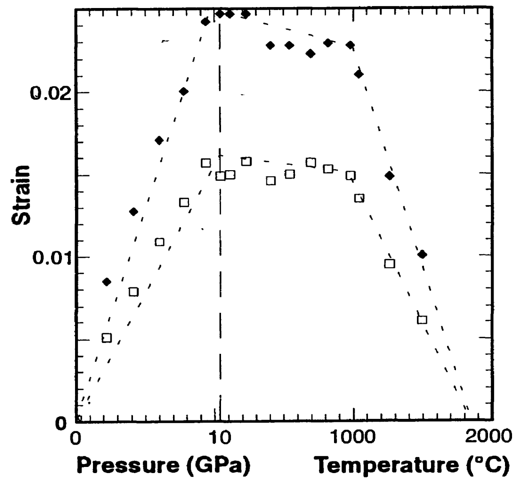

Fig. 2. Deviatoric strain determined from the broadening of the (111) diamond diffraction peak. The strain metric (relative units) is the square root of the difference in the squares of the full width at half maximum (open squares) and full width at quarter maximum (closed diamonds) of the high-pressure peak and the room condition peak, as calculated from the raw data. The strain increases linearly with pressure to the maximum reached. As temperature is increased, the cell pressure drops slightly, resulting in the small negative slope up to 1000°C with no evidence of sample yielding. Above 1000°, the relaxation of strain indicates ductile yielding as the strength of diamond falls below the deviatoric stress.

Both the starting material and the deformed sample were examined with transmission electron microscopy (TEM). In the starting material, the average dislocation density is low, $<10^7$ cm^{-2}. Many grains are flake-like, probably because of cleavage in the {111} plane (Fig. 4A). Some microcracks may also be present, although it is difficult to characterize them fully. The deformed sample exhibits a much higher dislocation density, by at least three orders of magnitude; the distribution of the dislocations appears rather uniform (Figs. 4, B and C). Two types of dislocations are observed in virtually every grain studied: long, straight dislocations preferentially in the ⟨110⟩ directions running through the entire crystallite (Fig. 4C) and an extremely high density of dislocation tangles (Fig. 4B).

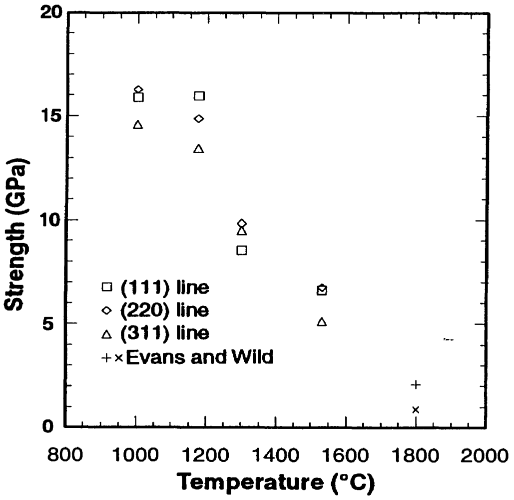

Fig. 3. Yield strength of diamond as a function of temperature, calculated from the multiplication of the strain-broadening of the indicated peaks by Young's modulus for diamond, 1050 GPa. The two points at 1800°C were measured at room pressure by a three-point bending method (*11*) and are for type I (+) and type II (×) diamonds. For temperatures below 1000°C, the sample clearly has not been yielded (see Fig. 2); therefore, the measurement at 1000°C may not represent the strength.

These microstructural features indicate that the sample is deformed in the ductile field by means of dislocations. The fact that there is no grain size reduction after deformation also suggests that brittle fracture or cataclastic flow as a ductile deformation mechanism does not make a significant contribution to the deformation. There is no evidence of graphitization in the deformed sample.

Previous studies on deformed diamonds revealed slip systems on cleavage plane {111}, namely ⟨110⟩{111} (6, *17*), giving five independent systems for crystal plasticity. However, the localized, strongly directional covalent bonding in diamond creates an exceptionally large lattice resistance to slip on all these slip systems under normal pressure and temperature conditions (*18*). DeVries showed that ductility can be enhanced by increasing pressure, on the basis of the onset of slip lines in single-crystal diamonds (*19*). The temperature at which the diamond begins to deform by crystal plasticity decreases from about 1500°C at 1 bar to <1000°C at 6 GPa. Our x-ray data indicate that ductile flow in the sample begins at ~1000°C and 10 GPa, in good agreement with the results of (*19*) and suggest that most of the dislocation movements occurred only at high temperatures.

This study demonstrates that our experimental technique for measuring yield strength can produce a deviatoric stress field sufficient to introduce yielding in even the most resistant materials. The deviatoric stress that can be generated by the compression of a loose diamond powder is found to be roughly twice the loading hydrostatic stress. The criteria for yield are clearly established: Yielding occurs as the stress redistributes once the yield strength of the most highly stressed grains is reached. Analysis by TEM of the recovered sample indicates that the dominant deformation mechanism is crystal plasticity.

The temperature dependence of the yield strength obviously defines limitations on industrial applications of diamond under pressure and temperature conditions. Knowledge of this dependence is also relevant in the study of inclusions in natural diamonds, especially in estimating pressure conditions under which the inclusions are formed, thus providing bounds for the depths from which the samples were brought (*20*). In particular, a few studies have suggested that some diamonds found in South Africa may have been brought up from the lower mantle and that the inclusions with compositions of (Mg,Fe) SiO_3 and $CaSiO_3$ may have been back-transformed from their perovskite-type structures under the pressure and temperature conditions (*21*). Indeed, with a yield strength of a few gigapascals at 1500°C, diamond cannot maintain enough pressure for the perovskite-structured (Mg,Fe)SiO_3 and $CaSiO_3$ to survive under pressure and temperature conditions in the upper mantle.

These results also have implications on the development of the next generation of high-pressure apparatus, with diamond as anvil material. If high pressure and high temperature are desired, then the strength of diamond will be highly compromised at temperatures above 1200°C, where its strength becomes weaker than that of tungsten carbide at room temperature. This limit suggests that internally heated, large volume systems that use sintered diamond anvils may provide higher pressures at these temperatures than do externally heated diamond anvil cells if yield strength is the limiting property.

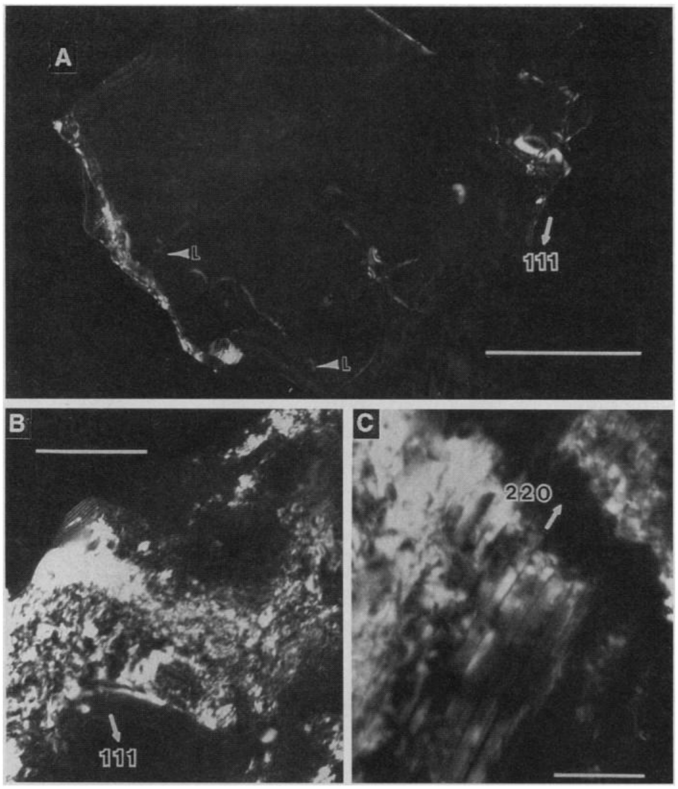

Fig. 4. Dark-field electron micrographs of diamond before and after the experiment. **(A)** Starting material. Some long, relatively straight dislocations are evident, indicating a previous history with a certain degree of plastic deformation. Free dislocation density is very low; because of the small grain size, only an upper bound can be estimated, namely 10^7 cm^{-2}. Some dislocation loops (L) are also present, which were probably formed during the diamond growth process. **(B)** Deformed sample. Note the high dislocation density, resulting in the steel-wool–like appearance. **(C)** Deformed sample. Tilting experiments indicate that the long, straight dislocations have Burgers vectors of the ⟨110⟩ type. The high density of dislocation tangles are out of contrast in this micrograph. Diffraction conditions are indicated for each micrograph. Scale bars indicate 0.5 μm.

REFERENCES AND NOTES

1. See, for example, H. K. Mao, P. M. Bell, K. J. Dunn, R. M. Chrenko, R. C. DeVries, *Rev. Sci. Instrum.* **50**, 1002 (1979).
2. See, for example, O. Shimomura, W. Utsumi, T. Taniguchi, T. Kikegawa, T. Nagashima, in *High-Pressure Research: Applications to Earth and Planetary Sciences*, Y. Syono and M. H. Manghnani, Eds. (American Geophysical Union, Washington, DC, 1992), pp. 3–11.
3. T. Kondo *et al.*, *High Temp. High Pressures* **25**, 105 (1993).
4. C. A. Brooks, *Nature* **228**, 660 (1970).
5. E. H. Hull and G. T. Malloy, *J. Eng. Indust.* **88**, 373 (1966).
6. T. Evans and R. K. Wild, *Philos. Mag.* **12**, 479 (1965).
7. T. Evans and P. F. James, *Proc. R. Soc. London Ser. A* **277**, 260 (1964).
8. P. W. Bridgman, *Studies in Large Plastic Flow and Fracture* (McGraw-Hill, New York, 1952); M. S. Paterson, *Experimental Rock Deformation: The Brittle Field* (Springer-Verlag, New York, 1978), p. 254.
9. D. J. Weidner, Y. Wang, M. T. Vaughan, *Geophys. Res. Lett.* **21**, 753 (1994).
10. For a description of the large-volume, high-pressure apparatus, see D. J. Weidner *et al.*, in (*2*), pp. 13–17. In the present experiment, the anvils are composed of sintered diamond, with 4 by 4 mm^2 truncations. Pyrophyllite gaskets are used to provide lateral support for the anvils. Weidner *et al.* [in (*2*)] also described cell assemblies used for high-pressure and high-temperature experiments. The cubic pressure medium is amorphous boron mixed with 20 weight epoxy, with a 6-mm edge length. Amorphous carbon is the heating element. A direct-current power supply provides a constant power input so that temperatures are stable within ±5° at ~1500°C. Temperatures in the sample are measured with $W_{0.95}Re_{0.05} - W_{0.74}Re_{0.26}$ thermocouples. The sample is under a uniform pressure environment with vertical temperature variations of less than 20°C at 1200°C in a 1.5-mm-long sample.
11. D. L. Decker, *J. Appl. Phys.* **42**, 3239 (1971).
12. The multichannel analyzer used in data collection is frequently calibrated with the characteristic decay energies of radioactive standards ^{57}Co, ^{129}I, and ^{109}Cd. Before and after each run, a mixture of Si, Al_2O_3, and MgO is placed in the diffraction volume and the positions of the diffraction peaks are used to calibrate the 2θ angle. This standard mixture also provides a direct calibration between the channel numbers and *d* spacings.
13. As discussed in (*9*), the microscopic stress in the sample can be generated by many mechanisms: anisotropic elastic properties in a hydrostatic macroscopic stress field, heterogeneous elastic properties in a hydrostatic macroscopic stress field, and the additional effects of a macroscopic deviatoric stress field. Theories regarding thermally induced stress in a polyphase aggregate made of anisotropic grains are applicable to the current problem. The results of previous studies [J. B. Walsh, *J. Geophys. Res.* **78**, 7637 (1973); W. Kreher, *J. Mech. Phys. Solids* **38**, 115

(1990); V. Tvergaard and J. W. Hutchinson, *J. Am. Ceram. Soc.* **71**, 157 (1988)] allow one to estimate properties of the microscopic deviatoric stress for particular material properties. These studies reveal that the microscopic stress varies within individual grains, but the grain size should not affect the amplitude of the microscopic stress field [A. G. Evans and D. R. Clarke, in *Thermal Stresses in Severe Environments*, D. P. H. Hasselman and R. A. Heller, Eds. (Plenum, New York, 1980), pp. 629–649].

14. M. H. Grimstitch and A. K. Ramdas, *Phys. Rev. B* **11**, 3139 (1975).
15. T. N. Loladze and G. V. Bockuchava, in *New Developments in Grinding*, First Proceeding of the International Grinding Conference (Carnegie Press, Pittsburgh, PA, 1972), pp. 432–448.
16. B. Evans and C. Goetze, *J. Geophys. Res.* **84**, 5505 (1979).
17. T. Evans and M. Omar, *Philos. Mag.* **7**, 843 (1953).
18. See, for example, H. J. Frost and M. F. Ashby, *Deformation-Mechanism Map: The Plasticity and Creep of Metals and Ceramics* (Pergamon, New York, 1982), p. 166.
19. R. C. DeVries, *Mater. Res. Bull.* **10**, 1193 (1975).
20. M. Schrauder and O. Nevon, *Nature* **365**, 42 (1993).
21. B. H. Scott-Smith, R. V. Danchin, J. W. Harris, K. J. Stracke, in *Kimberlites I: Kimberlites and Related Rocks*, vol. 11A of *Developments in Petrology*, J. Kornprobst, Ed. (Elsevier, Amsterdam, 1984), pp. 121–142. Also see S. E. Kessen and J. D. Fitz Gerald, *Earth Planet. Sci. Lett.* **111**, 229 (1991).
22. Supported by National Science Foundation grant EAR9219245.

31 May 1994; accepted 24 August 1994

Vibrationally Coherent Photochemistry in the Femtosecond Primary Event of Vision

Qing Wang, Robert W. Schoenlein, Linda A. Peteanu,*
Richard A. Mathies, Charles V. Shank

Femtosecond pump-probe experiments reveal the impulsive production of photoproduct in the primary event in vision. The retinal chromophore of rhodopsin was excited with a 35-femtosecond pulse at 500 nanometers, and transient changes in absorption were measured with 10-femtosecond probe pulses. At probe wavelengths within the photoproduct absorption band, oscillatory features with a period of 550 femtoseconds (60 wavenumbers) were observed whose phase and amplitude demonstrate that they are the result of nonstationary vibrational motion in the ground state of the photoproduct. The observation of coherent vibrational motion of the photoproduct supports the idea that the primary step in vision is a vibrationally coherent process and that the high quantum yield of the cis→trans isomerization in rhodopsin is a consequence of the extreme speed of the excited-state torsional motion.

The first step in vision, the light-induced isomerization of the retinal chromophore in rhodopsin, is complete in only 200 fs, making it one of the fastest photochemical reactions (*1*–*3*). Our previous studies suggested that coherent nuclear motion might accompany this ultrafast, highly efficient (quantum yield = 0.67) reaction because the 200-fs reaction time is comparable to or less than the period of torsional vibrations of the retinal chromophore (*4*). Does vibrational coherence play an important role in the first step in vision? Femtosecond optical techniques provide a powerful tool for examining the role of vibrational coherence in ultrafast reactions by creating coherent states of matter that reflect the motion of individual molecules. We report the observation of coherent vibrational motion in the photoproduct of the ultrafast isomerization in rhodopsin. Our results indicate that the isomerization proceeds along a diabatic pathway connecting the excited state of the 11-cis reactant with the ground state of the all-trans photoproduct (Fig. 1). The coherent nuclear dynamics observed here reveal the intimate connection between the speed of the cis→trans isomerization in rhodopsin and its photochemical quantum yield, thereby establishing a new paradigm for the photochemistry of vision.

Vibrational coherence is a natural consequence of nonstationary vibrational states excited by femtosecond optical pulses [see (*5*)] and can result from at least three elementary processes (*6*). First, coherent vibrational motion of the reactant in the ground state can be produced by femtosecond excitation through stimulated Raman scattering. For example, nonstationary ground-state vibrational motion has been observed in molecular crystals (*7*) and in the biological pigment bacteriorhodopsin (*6*, *8*). Second, vibrational coherence can be produced on the excited-state potential energy surface and has been observed in a variety of dye molecules in solution (*9*), in small molecules in the gas phase (*10*, *11*), and in bacteriorhodopsin (*12*). Recently, excited-state vibrational coherence has also been observed in photosynthetic reaction centers (*13*). The third case is where vibrational coherence persists throughout the time course of a photochemical reaction and is observed in the product. This case is the most interesting because it elucidates the role of nonstationary states in the ultrafast reaction dynamics. Such coherence has been observed in the ultrafast photodissociation of I_3^- (*14*). We show here that coherent nuclear vibrations can also be observed in the product of an ultrafast photochemical reaction that occurs within a protein at room temperature.

Rhodopsin samples were prepared from bovine retinas and dissolved in Ammonyx LO detergent solution as described previously (*1*). Femtosecond pump-probe measurements were performed with 35-fs pump pulses at 500 nm, and transient changes in absorption were measured from 450 to 570 nm with 10-fs blue probe pulses and from 560 to 640 nm with 10-fs red probe pulses. The method for generating 35-fs pump pulses at 500 nm as well as 10-fs probe pulses is described elsewhere (*15*). The experimental configuration used to obtain time-resolved differential transmission spectra was identical to that used in previous experiments. The average pump power was ~3 μW at a repetition rate of 540 Hz. The pump (~0.5 mJ/cm^2) and probe (~0.04 mJ/cm^2) beams were focused in a 0.3-mm jet of flowing bovine rhodopsin (15 OD/cm). The flow rate was

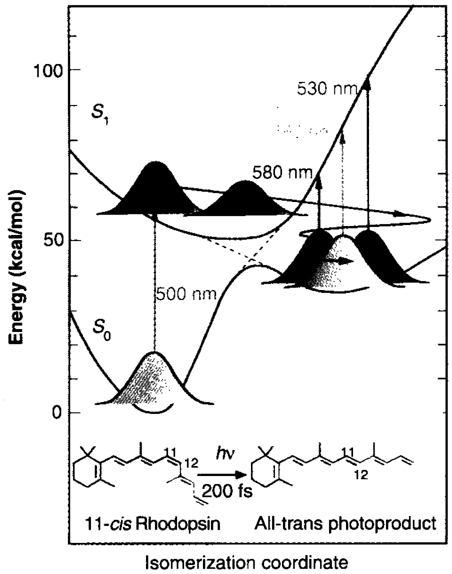

Fig. 1. Schematic potential energy surfaces for the femtosecond isomerization of rhodopsin after optical excitation of the molecule from the ground state S_0 to the excited state S_1. The wave packets in the photoproduct potential well illustrate how ground-state vibrational motion effects the photoproduct absorption. The dashed lines indicate the diabatic pathway along which the reaction proceeds.

Q. Wang and C. V. Shank, Materials Sciences Division, Lawrence Berkeley Laboratory, and Department of Chemistry, University of California, Berkeley, CA 94720, USA.

R. W. Schoenlein, Materials Sciences Division, Lawrence Berkeley Laboratory, Berkeley, CA 94720, USA.

L. A. Peteanu and R. A. Mathies, Department of Chemistry, University of California, Berkeley, CA 94720, USA.

*Present address: Department of Chemistry, Carnegie Mellon University, Pittsburgh, PA 15213, USA.